Tracking Hole Transport in DNA Hairpins Using a Phenylethynylguanine Nucleobase

Kristen E. Brown, Arunoday P. N. Singh, Yi-Lin Wu, Ashutosh Kumar Mishra, Jiawang Zhou, Frederick D. Lewis,* Ryan M. Young,* and Michael R. Wasielewski*

Department of Chemistry, Argonne-Northwestern Solar Energy Research (ANSER) Center, and Institute for Sustainability and Energy at Northwestern, Northwestern University, Evanston, Illinois 60208-3113, United States

* Supporting Information

ABSTRACT: The hole transport dynamics of DNA hairpins possessing a stilbene electron acceptor and donor along with a modified guanine (G) nucleobase, specifically 8-(4′-phenylethynyl)deoxyguanosine, or EG, have been investigated. The nearly indistinguishable oxidation potentials of EG and G and unique spectroscopic characteristics of $EG^{+\bullet}$ make it well-suited for directly observing transient hole occupation during charge transport between a stilbene electron donor and acceptor. In contrast to the cation radical $G^{+\bullet}$, $EG^{+\bullet}$ possesses a strong absorption near 460 nm and has a distinct Raman-active ethynyl stretch. Both spectroscopic characteristics are easily distinguished from those of the stilbene donor/acceptor radical ion chromophores. Employing EG, we observe its role as a shallow hole trap, or as an intermediate hole transport site when a deeper trap state is present. Using a combination of ultrafast absorption and stimulated Raman spectroscopies, the hole-transport dynamics are observed to be similar in systems having EG vs G bases, with small perturbations to the charge transport rates and yields. These results show EG can be deployed at specified locations throughout the sequence to report on hole occupancy, thereby enabling detailed monitoring of the hole transport dynamics with base-site specificity.

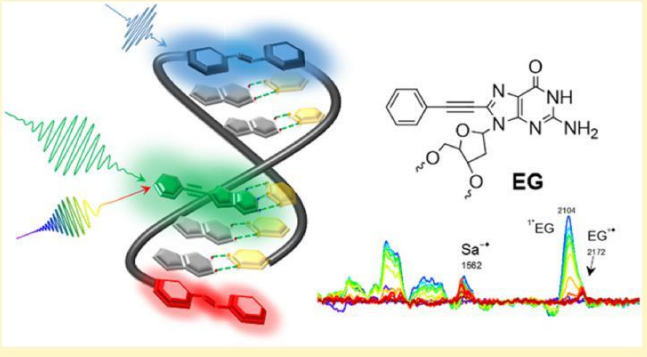

INTRODUCTION

The observation of wirelike charge transport in duplex DNA[1−3] has prompted extensive, careful design of DNA sequences, specifically tailored to achieve high-efficiency hole transport. Substitution of diblock polypurine sequences in lieu of naturally occurring purine-pyrimidine mixed sequences has led to significantly higher efficiencies for photoinduced charge transport[4,5] as has modification to natural base pairs.[6−9] Of particular interest is the role of guanine, which has the lowest oxidation potential of the natural nucleobases.[10,11] As such, guanine acts as a shallow hole trap that can influence the dynamics of competitive charge recombination and charge transport in DNA. Chemical reactions of the guanine cation radical can also lead to DNA strand cleavage,[12,13] and studies of photoinduced oxidative strand cleavage in duplexes containing multiple G-C base pairs by Barton, Schuster, and Giese in the 1990s led to the current models for hole hopping in DNA.[14−16]

While previous studies have demonstrated efficient hole transport in G-tracts across series of A_mG_n diblock purine sequences,[4] mechanistic understanding of these systems relies on a detailed kinetic analysis of the donor and acceptor signals. In particular, direct detection of oxidized intermediates, specifically the guanine cation ($G^{+\bullet}$), remains challenging. Electronic absorption spectroscopy has, until recently, been limited to studies of the more stable, neutral radical $(G\text{-}H)^{\bullet}$ generated by flash photolysis following one-electron oxidation by the sulfate radical anion ($SO_4^{-\bullet}$).[17,18] Kobayashi and Tagawa have reported the transient absorption spectra of $G^{+\bullet}$ formed upon pulse radiolysis-transient absorption of several duplexes containing one or more G:C base pairs and its deprotonation to form the more stable neutral radical $(G\text{-}H)^{\bullet}$. Both reactive intermediates have broad, weak transient spectra in the 350−700 nm region with no characteristic absorption bands.[19]

Our recent work[20] using a diphenylacetylenedicarboxamide hole donor revealed a weak $G^{+\bullet}$ absorption in the visible spectrum, where it is typically obscured by the much stronger and broader absorption features of the chromophores typically employed in these studies.[21] Moreover, it was demonstrated that the already weak intensity further decreases with the length of the purine-tract in which it is embedded, which makes directly tracking the specific location of the photoinjected hole quite challenging.

To overcome these issues, we recently synthesized and studied an electron-rich guanine derivative, 8-(4′-aminophenyl-ethynyl)guanine, GEAn, which provided evidence of hole delocalization in a G-quadruplex architecture using femto-

second transient absorption (fsTA) spectroscopy and femtosecond stimulated Raman spectroscopy (FSRS).[22] The addition of the aminophenylethynyl group to the 8-position of G results in a strong absorption band for the cation radical species, ca. 510 nm, with only a minor shift in the oxidation potential of the G unit, making this species an excellent starting point for designing a spectroscopic tag to study hole transport dynamics within DNA.

Here, we aim to optically identify the role of intermediate hole acceptors in hairpin-forming DNA charge conduits through development of a synthetically modified guanine nucleobase analogue, specifically 8-(4′-phenylethynyl)-deoxyguanosine, EG (Chart 1a). We observe a strong $EG^{+\bullet}$

Chart 1. Structures of (a) Sa, Sd, and EG and (b) the Hairpins in This Study[a]

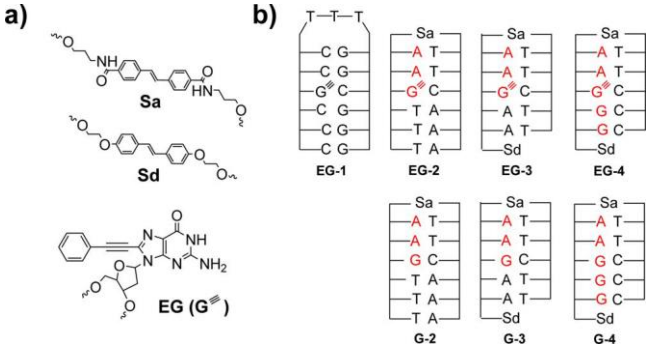

[a]Hole transfer pathway highlighted in red. The control compound EG-H_2 is the protonated version of EG.

absorption band at 460 nm, far removed from the congested bands in the 500−600 nm region of the spectrum of the stilbene-based donor and acceptor we have previously employed,[20] which thereby allows us to track the hole population directly. The similarity of the oxidation potential to G means that EG can be placed at a specific location within a G-tract and serve as a site-specific indicator of hole arrival, with minimal expected perturbation of the dynamics. In addition, the phenylethynyl group is strongly Raman active, which provides an alternative, base-specific approach to track the hole location using FSRS.

To provide direct spectroscopic evidence of EG as a hole acceptor, we incorporated EG into a series of DNA hairpins (Chart 1b), capped with a nonreactive thymine bridge (EG-1) or photooxidant stilbenedicarboximide (Sa) linker (EG-2). We also probe the role of EG in the presence of a deep hole trap (EG-3, -4), namely, stilbenediether (Sd). The stilbene linkers have been demonstrated to produce stable B-DNA hairpins and display distinct spectral tags.[23,24] We selected A_2G as the initial bridge based on the high quantum yield of charge separation (ca. 25%) in related systems.[4] The four hairpins were designed to (1) identify the spectral signature of $EG^{+\bullet}$ when employed as a (shallow) terminal trap state, (2) probe $EG^{+\bullet}$ as an intermediary acceptor state, and (3) distinguish $EG^{+\bullet}$ from $G^{+\bullet}$ within a hole transport conduit. Reference hairpins G-2-4 with G in place of EG were also studied to compare the dynamics and spectra. We find that, indeed, EG can serve as a site-specific probe of the hole location in these systems, and maintains similar transport and recombination behavior compared to sequences with unsubstituted G despite small differences in hole transport rates.

MATERIALS AND METHODS

Synthesis and characterization of 8-(4′-phenylethynyl)deoxyguanosine (EG-H_2), hairpins EG-1−4, G-1−4, and relevant reference compounds are provided in the Supporting Information (SI) along with experimental details for the time-resolved spectroscopies. A description of the fitting methodology and details of the applied kinetic models are also presented in the SI.

RESULTS AND ANALYSIS

Electrochemistry. Differential pulse voltammetry provides oxidation potentials of E_{ox} = 1.12 and 1.11 V vs SCE (0.1 M nBu_4NPF_6 in DMF) for EG-H_2 and deoxyguanosine, respectively (Figure S1), which are effectively the same within the instrumental resolution. The oxidation potential of the next most easily oxidized nucleobase, adenine, is higher by about 0.4 eV,[25] so the overall energetic landscapes of the EG-containing sequences remains similar to those with G. Any small shift in potential resulting from incorporation in the DNA hairpins is expected to only slightly perturb the hole transport dynamics, as discussed in detail below.

Steady-State Spectroscopy. Figure 1 shows the absorption spectra of the hairpins normalized at 260 nm and their

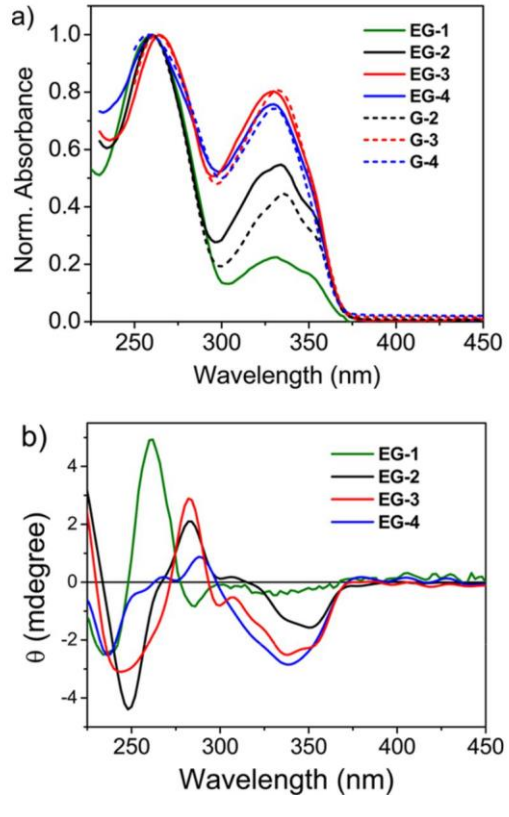

Figure 1. (a) UV/vis absorption spectra normalized to the 260 nm band and (b) circular dichroism spectra of EG hairpins (3 μM) in phosphate buffer (10 mM phosphate, 0.1 M NaCl, pH 7.2).

circular dichroism (CD) spectra. The UV spectrum of EG-1 reveals that the addition of the phenylethynyl substituent at the 8-position red-shifts the guanine ground-state absorption spectrum from 253 nm with a shoulder at 272−332 nm with a shoulder at 350 nm. The structured absorption spectrum is reminiscent of the L_a and L_b bands observed in guanine.[26,27] The EG absorption coincides with the Sa and Sd steady-state absorption, as is apparent in the spectra of EG-2−4. Each of

these Sa-containing hairpins shows an increase in the 330 nm absorption band relative to the 260 nm nucleobase absorption band. This increase is demonstrated in Figure S2 (SI) by comparison of the spectra of compounds EG-ref and Sa-ref which contain one EG or Sa chromophore, respectively, and 6 A:T base pairs.

The CD spectra of hairpins EG-2−4 indicates they adopt B-DNA structures similar to previously studied Sa-linked hairpins,[28] as evidenced by the sign and intensity pattern in the short-wavelength portion of the spectrum (200−300 nm). High values for the first derivatives of the thermal dissociation profiles for sequences EG-1−4 (CD-melting > 50 °C, Figure S3) indicates the phenylethynyl substituent at the 8-position of guanine enhances duplex stability, presumably by extending into the major groove without disrupting the base pairing. The bands in the long-wavelength region (300−400 nm) are attributed to induced CD of the two or three achiral chromophores which have absorption maxima in the same wavelength region of the CD minima.[28] In contrast, the EG-1 spectrum has a strong positive band at 260 nm and a negative band around 215 nm which indicate some distinct features of an A-DNA-like structure.[29] Poly(dG).poly(dC) sequences similar to that of EG-1 are known to form intermediate or mixed B/A type structures.[30,31] This structural difference should not compromise the utility of EG-1 as a model sequence designed to probe the behavior of EG in the absence of stilbene chromophores. The decreased intensity of the induced CD band of EG-1 is a consequence of the absence of the stilbene chromophores.

Transient Absorption Spectroscopy. Femtosecond transient absorption spectroscopy is used to initiate and monitor hole transport dynamics. Briefly, transient absorption spectra were acquired after 350 nm excitation followed by a broadband visible-to-NIR probe. At the excitation wavelength of 350 nm, we expect an approximate 2:1 Sa:EG coexcitation ratio. The normalized absorption of EG-2 and EG-3, the latter of which contains both stilbene chromophores, reveals that Sd also contributes to 18% of the total absorption at 350 nm, but is not expected to impact the hole transport properties of the system.[32] In these systems, the fraction of absorbed photons leading to the population of ^{1}*Sa from which hole injection occurs is approximately 0.55 (see Figures 1 and S2). All samples were purged with N_2 and stirred to minimize the effects of degradation and local heating.

We first investigated the excited-state behavior of the EG-H_2 chromophore in methanol, shown in Figure 2a. Excitation of EG at 350 nm results in a sharp excited-state absorption band at 500 nm which extends well into the near-infrared region with two small maxima at 1000 and 1250 nm. The signal decays biexponentially with τ_1 = 6 ps and τ_2 = 18 ps, with minimal spectral evolution. The relaxation dynamics are largely similar when EG is placed into a duplex hairpin, as in EG-1 (Figure 2b): the maximum absorption shifts to 505 nm, and the biexponential decay is somewhat slower (9 and 27 ps). The location of the 505 nm absorption is reminiscent of the $GEAn^{+\bullet}$ absorption; however, the similarity of the spectra and dynamics of EG-1 with those of the isolated EG-H_2 strongly suggests that the 505 nm band belongs to ^{1}*EG and that there is no charge transfer or strong exciplex interaction between the EG and the neighboring C:G base pairs.

The fsTA spectra for EG-2−3 and G-2−3 following 350 nm excitation are shown in Figures 3 and S4, respectively. The spectra are dominated initially by the absorption of the ^{1}*Sa

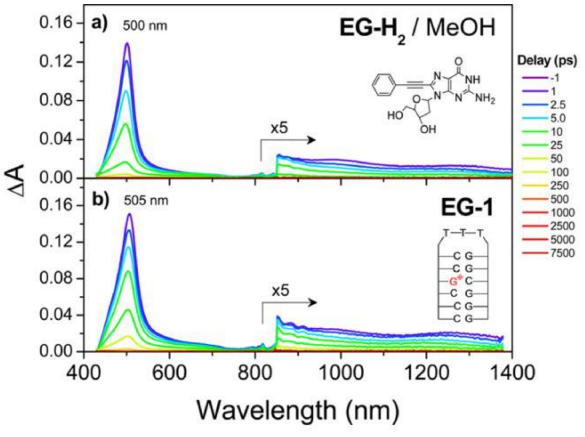

Figure 2. Femtosecond transient absorption spectra for (a) EG-H_2 in methanol and (b) EG-1 in aqueous buffer acquired after 350 nm, 500 μJ excitation. The excited-state maxima of ^{1}*EG in both occur near 500 nm, and decay biexponentially. Delays are given in ps.

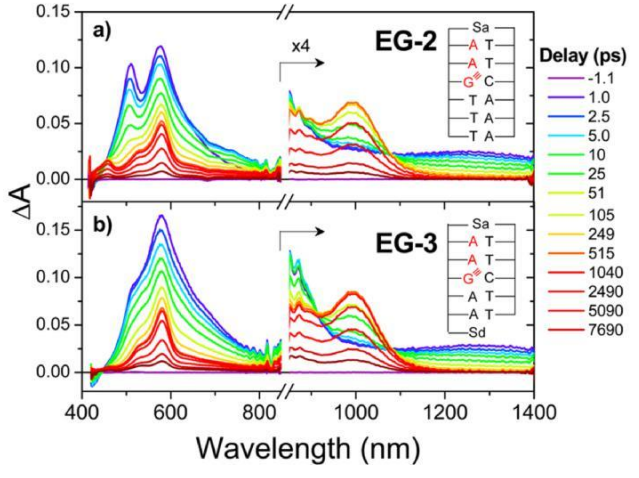

Figure 3. Femtosecond transient absorption spectra of (a) EG-2 and (b) EG-3 following 350 nm excitation. Delays are given in ps. Early time traces (blue) represent the EG excited state (λ_{max} = 510 nm) and ^{1}*Sa excited state (λ_{max} = 578 nm). At late times, absorption maxima of $EG^{+\bullet}$ (λ_{max} = 460 nm) and $Sa^{-\bullet}$ (λ_{max} = 577 and 1000 nm) are apparent.

state at 577 nm.[33] Coexcitation of EG is evidenced by the narrow 510 nm band of ^{1}*EG that is likely shifted by added absorption at redder wavelengths by ^{1}*Sa. Over the next tens of picoseconds, the 577 nm band sharpens, characteristic of $Sa^{-\bullet}$,[33] and new bands at 460 and 1000 nm appear. The 1000 nm band is also assigned to absorption by $Sa^{-\bullet}$ as it appears concomitantly with the 577 nm $Sa^{-\bullet}$ band in G-2 where there are no additional chromophores.

We assign the new 460 nm feature that appears at later times to absorption by $EG^{+\bullet}$, since it appears with the same rate as the bands belonging to $Sa^{-\bullet}$ and is also absent in the reference sequences G-2−4 (Figure S4). The shift of the 460 nm $EG^{+\bullet}$ band relative to the guanine-quadruplex $GEAn^{+\bullet}$ band plausibly results from the decreased conjugation length owing to replacement of the aniline moiety with a phenyl substituent.[22]

To model the hole transport dynamics in EG-2, we employ global kinetic analysis with the simplified model depicted in Scheme 1a. Excitation of the Sa-containing hairpins results in relaxation (k_R) followed by charge separation (k_{CS}) to form $Sa^{-\bullet}/EG^{+\bullet}$. As explicit separation of the ^{1}*EG and ^{1}*Sa (and

Scheme 1. Kinetic Scheme for Hole Transport in (a) EG-2 (Sa-A_2-EG-T_3) and (b) EG-3 (Sa-A_2-EG-A_2-Sd) and EG-4 (Sa-A_2-EG-G_2-Sd)[a]

a)

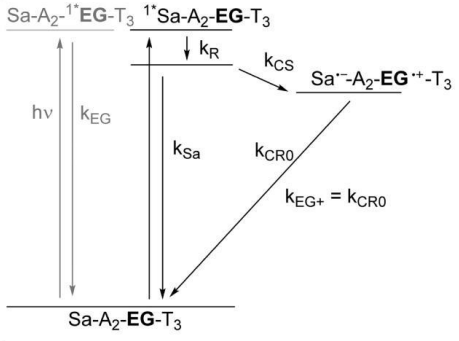

b)

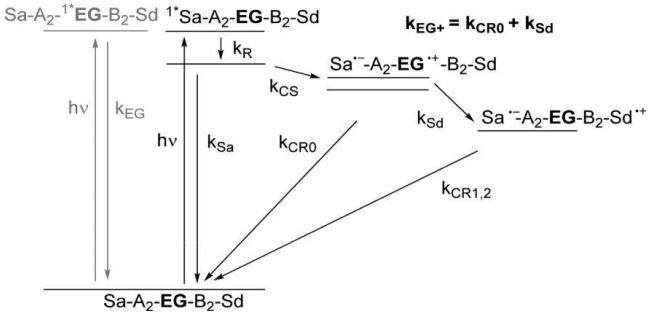

[a]Coexcitation of EG and Sa is followed by relaxation/fluorescence from ^{1}*EG and ^{1}*Sa, and reversible hole injection from ^{1}*Sa to form $Sa^{-\bullet}$-A^+, all of which are captured in part by k_R. Hole transport to EG occurs with rate k_{CS}; the higher energy level in this state represents EG-3 with the bridge $B_2 = A_2$, while the lower energy state represents EG-4 with the bridge $B_2 = G_2$. In EG-3−4 the rate (k_{Sd}) and yield of trapping by $Sd^{+\bullet}$ are determined by the sequence of intervening base pairs B: either A_2 or G_2. States in gray are not captured by the data modelling. Similar schemes hold for G-2 (Sa-A_2-G-T_3) and for G-3 (Sa-A_2-G-A_2-Sd) and G-4 (Sa-A_2-G-G_2-Sd).

^{1}*Sd) populations leads to a large number of parameters in the model, we simplify the kinetic model to assume a single excited-state population.[34] Based on the data for EG-1, the initial dynamics during the first ~100 ps will thus contain some evolution from the secondary ^{1}*EG population. This observation is corroborated by FSRS measurements discussed below. However, since hole transport primarily occurs after this early period, the simplified kinetic model should serve as a good approximation to those long-time dynamics. Details of the kinetic modeling and results can be found in SI section 3, and kinetic parameters are summarized in Table 1.

For EG-2, global analysis of the fsTA data captures the initial decay of the ^{1}*EG and ^{1}*Sa populations with one process, τ_R ~ 7 ps. This relaxation comprises the initial decay of ^{1}*EG observed in EG-1, along with some of the reversible hole injection (^{1}*Sa ⇌ $Sa^{-\bullet}$) observed when stilbenedicarboxamide is used as a hole donor and A:T base pair as hole acceptor.[35] The species-associated spectrum (SAS, Figure S8) for this state, a combination of ^{1}*EG and ^{1}*Sa ⇌ $Sa^{-\bullet}$, supports this assignment. A similar spectrum and rate are obtained for G-2, without the 505 nm contribution from ^{1}*EG. This composite state then decays to form the $Sa^{-\bullet}/EG^{+\bullet}$ charge-separated state in τ_{CS} = 51 ps, as indicated by the appearance of the 460 nm band. The $Sa^{-\bullet}/EG^{+\bullet}$ state then decays in τ_{EG+} = 3.4 ns, while in G-2 the $Sa^{-\bullet}/G^{+\bullet}$ state decays in τ_{G+} = 1.4 ns. Nanosecond transient absorption (nsTA) spectroscopy reveals the same decay kinetics on the ns-μs time scale (Figures S17 and S20), and shows the evolution to a low intensity, much longer-lived 8 μs species with an absorption maximum at 440 nm. This species is most likely the ^{3}*Sa state, as the triplet state of unsubstituted trans-stilbene has an absorption maximum at ca. 390 nm in viscous solution at room temperature.[36] The presence of the similar band in G-2 also indicates that the band does not originate from EG.

The EG-2 kinetics inform the hole transfer dynamics in sequences EG-3−4, with Sd as the deeper hole trap. In both EG-3 and EG-4, the decreased initial intensity of the 505 nm ^{1}*EG band relative to that in EG-2 is attributed to competitive absorption by Sd (Figures 1 and S2). The spectra for both EG-3 and G-3 (Figure S4) are similar to those for EG-2 and G-2, respectively, with the initial appearance of the ^{1}*Sa and ^{1}*EG bands followed by the formation of the $Sa^{-\bullet}/EG^{+\bullet}$ radical pair. Despite the expected slower recombination from $Sa^{-\bullet}/EG^{+\bullet}$ for EG-3, the fsTA data (Figure 3b) do not clearly exhibit the 533 nm absorption associated with $Sd^{+\bullet}$ within the first 7 ns.

To model the charge separation and recombination processes, we extend the same kinetic model used above, allowing the possibility of hole trapping from the $Sa^{-\bullet}/EG^{+\bullet}$ state to form $Sa^{-\bullet}/Sd^{+\bullet}$ with rate k_{Sd} (Scheme 1b). The additional process changes the rates of decay of $EG^{+\bullet}$ and $G^{+\bullet}$ to

$$k_{EG+} = k_{CR0} + k_{Sd} \quad (1a)$$

$$k_{G+} = k_{CR0} + k_{Sd} \quad (1b)$$

where k_{CR0} is the value of k_{EG+} for EG-2 and represents the charge recombination from $EG^{+\bullet}$. A similar situation exists for

Table 1. Time Constants and Φ_{Sd} Derived from Global Fits of the fs/nsTA Datasets to the First-Order Kinetic Model Presented in Scheme 1[a]

	τ_R, ps[b]	τ_{CS}, ps[b]	τ_{EG+} (τ_{G+}) ns[b]	τ_{Sd}, ns[b]	τ_{CR1}, ns[c]	τ_{CR2}, μs[cf]	Φ_{Sd} (5 ns)	Φ_{Sd} (7 ns)[b]	Φ_{Sd} (10 ns)[c]	Φ_{Sd} (40 ns)[d]
EG-2	7.0 ± 0.3	51 ± 1	3.41 ± 0.01							
EG-3	1.7 ± 0.3	34 ± 1	2.74 ± 0.04	14 ± 1	5.8 ± 0.6	7.1 ± 0.6	<1%	<1%	<1%	<1%
EG-4	3.6 ± 0.3	37 ± 1	1.92 ± 0.04	4.4 ± 0.2	23 ± 1	3.0 ± 0.1	0.16	0.16	0.15	0.05
G-2	5.0 ± 0.3	40 ± 1	1.40 ± 0.01							
G-3	2.9 ± 0.3	39 ± 1	1.29 ± 0.01	16 ± 2	~1000		0.05	0.03	0.06	0.03
G-4	7.16 ± 0.3	57 ± 1	0.86 ± 0.02	2.2 ± 0.1	7.2 ± 0.2	0.7 ± 0.1	0.26[e]	0.21	0.20	0.07

[a]$\tau_X = (k_X)^{-1}$. Uncertainties are reported as the standard errors of the fits. Explicit decay pathways to the ground state are neglected, such that each time constant represents an effective time. [b]Determined from fsTA data. [c]Determined from nsTA data. [d]Value corrected for contamination by ^{3}*Sd by subtracting the spectrum at 40 μs. [e]Reference value taken from ref 4 and corrected for the fraction of Sa extinction coefficient at 350 nm (η_{Sa} = 0.75). [f]May include other decay pathways; see the SI.

.

G-2−4 with k_{G+} for charge recombination from $G^{\bullet+}$. For EG-3, charge separation occurs with a ~ 35 ps time constant to populate the $Sa^{-\bullet}/EG^{+\bullet}$ state, with absorption bands around 460, 577, and 1000 nm. This state decays with minor spectral changes; however, a small signal persists beyond the ~8 ns window of the fsTA experiment. The measured decay time of $Sa^{-\bullet}/EG^{+\bullet}$ is 2.7 ns in EG-3, which is faster compared to that in EG-2 (3.4 ns), suggesting a possible hole trapping pathway. The nsTA data (Figures S16−S23) show that the remaining population at long times largely decays over the next 5.8 ns (charge recombination) to a long-lived signal around 530 nm (Figure 4a), near the expected absorption of $Sd^{+\bullet}$.[37]

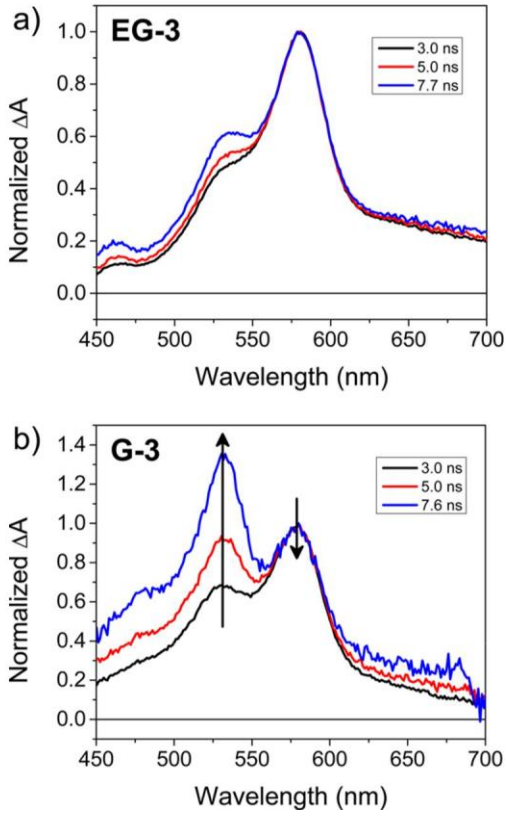

Figure 4. Normalized fsTA spectra for (a) EG-3 and (b) G-3 at long times showing the inversion of the 533 and 577 nm bands. Data are normalized to the $Sa^{-\bullet}$ absorption at 577 nm.

The spectra at long times (≫10 μs) do not show absorption from $Sa^{-\bullet}$ as would be expected for the fully charge-separated state. Instead, the 440 nm feature is reminiscent of the ^{3}*Sa spectrum. The rapid disappearance suggests that it decays by triplet−triplet energy transfer to a lower lying triplet state. In this case, the isolated 530 nm absorption feature could be the $T_n \leftarrow T_1$ transition of ^{3}*Sd.[36] However, it is also possible that some permanent oxidation of Sd is occurring due to incomplete removal of oxygen, resulting in a long-lived $Sd^{+\bullet}$ population that is not accompanied by the $Sa^{-\bullet}$, resulting in the 530 nm absorption band.

In G-3, there is more direct spectral evidence for hole trapping in low yield. After fast relaxation, charge separation occurs in 39 ps, followed by a 1.3 ns decay. Figure 4b shows that at long delays (3−7 ns), inversion of the 533 and 577 nm signal is observed. The low amplitude of the signal results from fast (1.3 ns) recombination.

The fsTA data for EG-4 and G-4 are both shown in Figure 5. Initially, the spectra appear similar to those of the hairpins

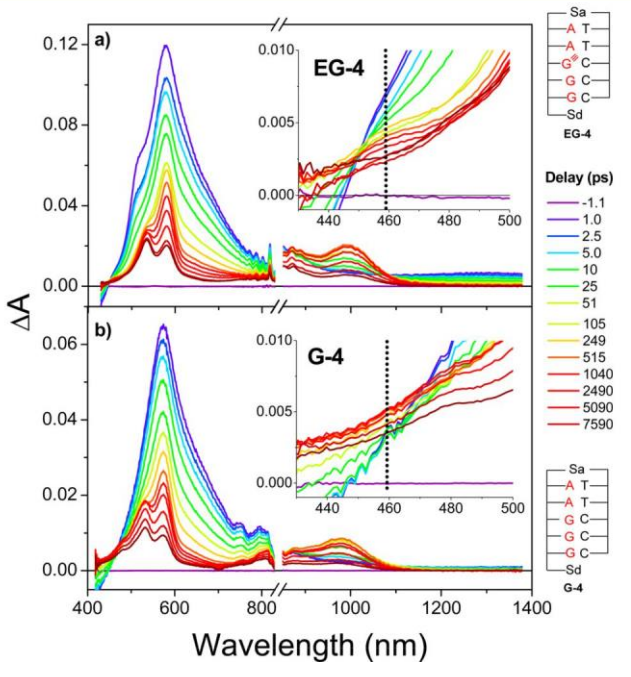

Figure 5. fsTA spectra of (a) EG-4 and (b) G-4 following 350 nm excitation. Delays are given in ps. At long delays hole trapping at $Sd^{+\bullet}$ in moderate yields is observed at 480 and 533 nm. Inset: Increased amplitude near 460 nm at intermediate (20−1000 ps) delays shows the characteristic absorption of $EG^{+\bullet}$ in EG-4 indicating the transit of the hole through EG before trapping at Sd.

discussed above. However, at long delays, we observe an increase in the absorption near 533 nm, characteristic of the $Sa^{-\bullet}/Sd^{+\bullet}$ pair. At intermediate times in EG-4 we observe an increased intensity near 460 nm, presumably owing to absorption by transiently oxidized EG before the rise of the $Sd^{+\bullet}$ band (Figure 5a, inset); a feature not observed in G-4 (Figure 5b, inset). The noticeable inversion of the 533 and 577 nm bands occurs after 2 ns, indicating a significant yield of hole trapping within the experimental window.

The kinetic processes are modeled as previously discussed. The lifetime of the $Sa^{-\bullet}/EG^{+\bullet}$ intermediate state in EG-4 is 1.9 ns, compared to the longer 3.4 ns lifetime in EG-2, which again suggests the presence of an additional decay pathway. The characteristic $Sa^{-\bullet}/Sd^{+\bullet}$ spectrum decays with τ_{CR1} = 23 ns. A second, slower recombination event is observed with τ_{CR2} = 3 μs, as evidenced by the similar species-associated spectrum with characteristic $Sa^{-\bullet}/Sd^{+\bullet}$ features. This process may arise from minor dynamical conformation(s) which disfavor charge recombination. Following the slower charge recombination, we observe the same low-amplitude signal at 530 nm as in EG-3. The reference sequence G-4 exhibits similar kinetics to those of EG-4, with the decay of the $Sa^{-\bullet}/G^{+\bullet}$ intermediate occurring with a time constant of 860 ps, compared to 1400 ps for G-2. Multiple recombination times are also observed by nsTA, with τ_{CR} = 7.2 and 650 ns, although the amplitude of the slower component is low (Figure S22).

Femtosecond Stimulated Raman Spectroscopy. FSRS data were acquired with a 350 nm actinic pump, and a ps Raman pump/fs broadband probe pair. The Raman pump wavelength (λ_{RP}) was tuned to 480 nm to be close to resonance

with the ^{1}*EG and EG$^{+\bullet}$ transitions. We also utilized a 600 nm Raman pump to resonantly enhance ^{1}*Sa and Sa$^{-\bullet}$ signals to track the hole injection process. FSRS spectra of EG-1 (Figure 6a), collected using λ_{RP} = 480 nm to resonantly enhance ^{1}*EG,

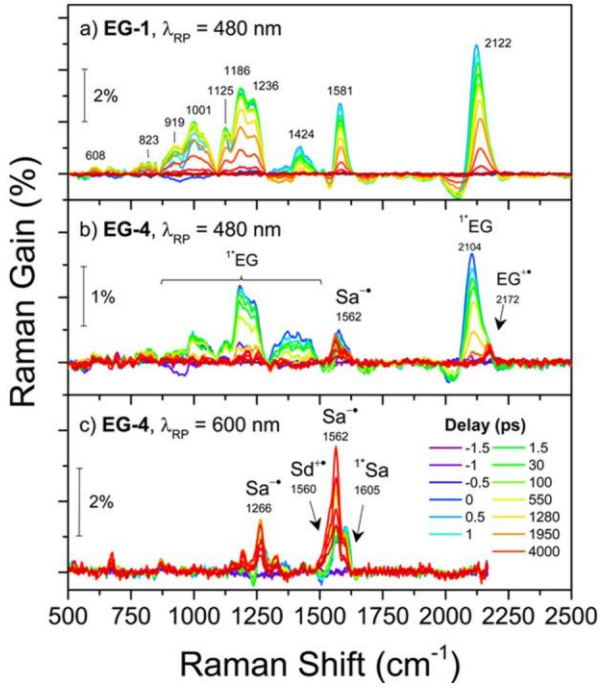

Figure 6. FSRS spectra of EG-1 and 4 following 350 nm excitation. (a) Spectra of EG-1 acquired with λ_{rp} = 480 nm. (b) Spectra of EG-4 (λ_{RP} = 480 nm) showing ^{1}*EG at early times and composite spectra of EG$^{+\bullet}$ and Sa$^{-\bullet}$ at late times. (c) Spectra of EG-4 acquired with λ_{RP} = 600 nm showing ^{1}*Sa at early times and Sa$^{-\bullet}$ at late times. Delay times are provided in ps. See the SI for mode assignments.

reveal several excited-state bands between 500 and 2200 cm^{-1} which all decay biexponentially. Time constants are similar to those determined by transient absorption spectroscopy. The absence of a time-dependent shift in the C C stretching mode at 2122 cm^{-1} corroborates the lack of charge separation in EG-1. Selected Raman mode assignments are given in the SI. In hairpins EG-2−4, the 480 nm Raman pump wavelength is also resonant with the transient EG$^{+\bullet}$ absorption. At early times, EG-2 closely matches EG-1, with low intensity peaks indicative of Sa$^{-\bullet}$ in the 1500−1600 cm^{-1} region forming at later times (Figure S25). The C C mode shifts to higher frequency (2172 cm^{-1}) following oxidation of EG, which directly indicates hole transfer to form EG$^{+\bullet}$.[22]

Raman spectra for EG-3 are provided in Figure S25, while those for EG-4 are provided in Figure 6b. The C C mode of ^{1}*EG initially following excitation appears at 2104 cm^{-1}. At late times, the spectra closely match those of EG-2 indicating similar hole transfer to EG$^{+\bullet}$. In contrast to EG-2, the early time spectra in the 1100−1500 cm^{-1} region are broadened with additional peaks between 1300 and 1500 cm^{-1} and decreased relative intensity of the 1175 cm^{-1} bands.

We also probe the dynamics of hole injection using a 600 nm Raman pump. Representative spectra for EG-4 are shown in Figure 6c, showing peaks at 1266, 1562, and 1605 cm^{-1}. After 35 ps, coinciding with the formation of the Sa$^{-\bullet}$/EG$^{+\bullet}$ state, the 1605 cm^{-1} mode becomes less pronounced. The appearance of the 1605 cm^{-1} mode as a small shoulder on the 1560 cm^{-1} band suggests its attribution to ^{1}*Sa. The DFT-calculated Raman spectra identify the 1605 cm^{-1} feature as the amide stretch of ^{1}*Sa, and the 1266 and 1562 cm^{-1} bands as the vinyl bending and stretching modes, respectively, of Sa$^{-\bullet}$ (Figure S38). In EG-4, there is a long-lived population with a peak at 1560 cm^{-1} that is consistent with the vinyl C C stretches in both Sa$^{-\bullet}$ and Sd$^{+\bullet}$ (see SI, Figures S39−40), which keeps with the modeling of the transient absorption data.

DISCUSSION

Ethynylguanine Absorption and Relaxation. The similarity between the EG-1 and the isolated EG-H$_2$ nucleoside dynamics and the lack of significant spectral evolution (Figure 1) strongly indicate that electron transfer or other photo-processes do not occur between ^{1}*EG and the adjacent C:G base pair in EG-1. The observed dynamics, thus, are the excited-state decay of ^{1}*EG. It is not unexpected that the addition of the phenylethynyl substituent at the 8-position would perturb the relaxation dynamics of unsubstituted guanine.[26] Increased radiative decay times have been observed in nucleobases modified such that torsion is restricted around nuclear coordinates that gate nonradiative decay via a conical intersection.[38] The vertical excited state may also quickly relax to a configuration where internal conversion is slowed, such as through an intramolecular charge transfer state as was shown in a recent theoretical study of 8-vinylguanine.[39] Additional work is necessary to identify the nature of biexponential decay in EG-H$_2$ and is beyond the scope of the current investigation. Importantly, however, parallel excitation of EG along with Sa appears to result in a short-lived population of ^{1}*EG that does not undergo charge transfer, and thus should not greatly alter the hole transport dynamics originating from ^{1}*Sa.

Hole Injection and Charge Separation. The FSRS spectra, acquired at 600 nm to resonantly enhance the 600 nm ^{1}*Sa ⇌ Sa$^{-\bullet}$ absorption, indicate a reversible charge injection process. As seen in Figure 7, in the first few ps following excitation, we observe an apparent combination of ^{1}*Sa and Sa$^{-\bullet}$ Raman features. We have previously observed that hole injection from ^{1}*Sa into a neighboring A-block is reversible,[35] obstructing resolution of the hole injection step. The FSRS

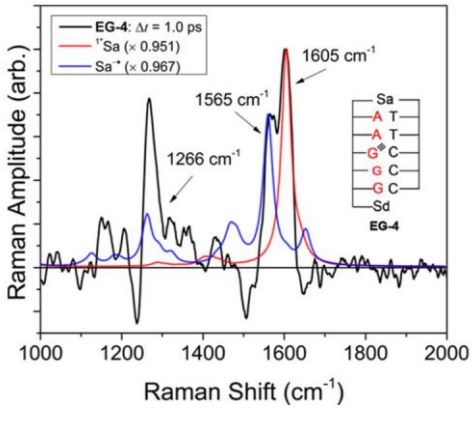

Figure 7. Comparison of the FSRS spectrum of EG-4 acquired at t = 1.0 ps (λ_{RP} = 600 nm) to the calculated spectra of ^{1}*Sa and Sa$^{-\bullet}$ at the B3LYP/6-31G* level with 15 cm^{-1} Lorentzian broadening. The feature at 1605 cm^{-1} is the amide stretch of ^{1}*Sa, while the peaks at 1266 and 1565 cm^{-1} are the vinyl bending and stretching modes of Sa$^{-\bullet}$, all of which are present at this delay due to the reversible charge injection.

spectra support this assessment. With a rapid pseudoequilibrium there will be sizable population of both species, as both possess an electronic transition at this Raman pump wave-length, until the population drains into a lower energy state, in this case $Sa^{-\bullet}/EG^{+\bullet}$ in the ~30 ps charge separation. Complete modeling of these processes is prohibitive, as discussed above, and so they are collectively captured with the relaxation pathway k_R. While not fully resolving these kinetics, the FSRS spectra offer a direct observation of the reversible injection process.

The rise in the $Sa^{-\bullet}$ signal also provides insight into the charge transport process in systems with a small A-block neighboring the donor. Direct kinetic comparison of the λ_{RP} = 480 nm and λ_{RP} = 600 nm Raman experiments for EG-2−4 (Figures S28−S30 and S33−S35, respectively) reveal nearly identical formation times for (isolated) $Sa^{-\bullet}$ and $EG^{+\bullet}$. This observation is consistent with a superexchange hole transport mechanism from Sa to $Sa^{-\bullet}/EG^{+\bullet}$. Under this mechanism, thought to occur for short A-tracts ($n < 3$),[40,41] the formation of $Sa^{-\bullet}$ and $EG^{+\bullet}$ should occur concomitantly and formation of the $Sa^{-\bullet}/A^{+\bullet}$ contact ion pair should not be spectrally or kinetically observable. In contrast, under a hopping mechanism, $Sa^{-\bullet}$ is fully reduced prior to hole transport from $A^{+\bullet}$ to $EG^{+\bullet}$, leading to different appearance times for the two species. We note, however, that the reversible hole injection discussed above may complicate the dynamics, and the true mechanism is likely more subtle.[42]

Hole Trapping Dynamics. The results of the kinetic modeling of the TA data offer insight into the hole transport dynamics and hole location in the EG- and G-sequences. As discussed above, charge separation in EG-2 occurs in 50 ps. This time, and the similar analogous time in G-2 are also close to the previously observed ~30 ps charge separation times for Sa-A_2 systems.[43] The discrepancy likely arises from the residual parallel decay of ^{1}*EG during this time range (Scheme 1a). As shown in Table 1, the extracted values for the hole trapping time τ_{Sd} are around 2 orders of magnitude larger than the charge separation times, despite the similar distances. This is likely a consequence of the different charge transport mechanisms at play depending on the number of intervening base pairs between the two radicals.[42]

Following charge separation, the $Sa^{-\bullet}/EG^{+\bullet}$ state decays in 3.4 ns, almost a factor of 2 slower than the G-2 reference sequence. The difference in recombination rates is likely a consequence of the slightly altered G_{CR} from the shift in oxidation potential of EG vs G, although contributions from altered electronic coupling between adjacent nucleobases cannot be ruled out. While the electrochemically determined oxidation potential of EG was measured to be the same as that of G, the difference in the potentials is likely exaggerated in the DNA medium. The dielectric environment is plausibly impacted by the neighboring nucleobases, lowering the effective dielectric constant relative to the highly polar DMF solvent used for electrochemical measurements. Additionally, the structure of the duplex in the region of the modified nucleobase may be perturbed as the phenylethynyl group protrudes into the major groove, possibly altering the oxidation potential and the electronic coupling. While the altered oxidation potential affects the recombination dynamics, the charge does not become irreversibly trapped at EG and does not prohibit using EG in the diblock architectures.

The behavior of $EG^{+\bullet}$ as a shallow hole trap can, in principle, be used to enhance the yield of charge separation in situations where recombination from the poly(purine) sequence outcompetes the deep hole trapping. By providing a site with an extended lifetime and lower recombination rate, more of the hole population can make its way to the deep trap state. While in EG-3 we do not see a strong rise in the characteristic signature of $Sd^{+\bullet}$, there are indications that the hole is transferring to the Sd trap site. At long-times (7.7 ns, Figure 4a), there is a weak growth of the 533 nm $Sd^{\bullet+}$ signal, though the amplitude suggests a < 1% trapping yield. The lifetime of the $Sa^{-\bullet}/EG^{+\bullet}$ charge-separated state in EG-3 is, however, significantly shorter than in EG-2, which indicates that there is a kinetic process competing with charge recombination. We calculate the hole transfer time from $EG^{+\bullet}$ to $Sd^{+\bullet}$, τ_{Sd} ($=1/k_{Sd}$), from eq 1, which for EG-3 gives τ_{Sd} = 13.9 ns. This rate would suggest as much as 40% (k_{Sd}/k_{EG+}) of the hole population can transfer to Sd. However, the 5.8 ns decay observed in the nsTA spectra indicates that the kinetics of charge recombination from the Sd trap are inverted, preventing any population from building up to a detectable level during the fsTA experiment, leading to the spectra observed in Figure 3b.

The situation is similar in G-3 where the $Sa^{-\bullet}/Sd^{+\bullet}$ radical pair is observed at long times, as seen in Figure 4a, although the observed yield is quite low. Kinetic analysis gives τ_{Sd} = 16.4 ns, but a maximum yield of only 8%. This low yield is independently corroborated by determining the yield directly from the spectra at a specific time. We calculate the yield of hole trapping on Sd, Φ_{Sd}, by obtaining the ratio of the ^{1}*Sa absorption amplitude at 500 fs and the area of the absorption at 7 ns delay and comparing that ratio to a known standard:[17]

$$\Phi_{Sd}(t) = \frac{A_{Sd^{+\bullet}}(t)}{A_{Sa^{1*}(t=0)}} \Big/ \frac{A_{Sa^{+\bullet}}(t)}{A_{Sa^{1*}_{ref}(t=0)}} \eta_{Sa}\Phi_{ref} \quad (2)$$

The coexcitation of the EG chromophore and the overlapping absorptions of ^{1}*EG and ^{1}*Sa requires a correction for the fraction of absorbed photons that lead to the formation of ^{1}*Sa (η_{Sa}). We take G-4 as the reference with Φ_{ref} = 26% when corrected for the fraction of Sa absorbing at 350 nm.[4] Further details are provided in SI section 3. This approach provides a time-dependent quantum yield of charge trapping, as the ratio is based on the area at a given time delay; Table 1 reports the yields calculated at 5 and 7 ns using the fsTA measurement, and 10 and 40 ns based on the nsTA data. Ideally, the yield would be reported when the trapping step is completed and the spectral intensity is effectively constant. However, as the trapping rate is on the same order as the charge recombination (τ_{EG+} and τ_{Sd} ~ 3 ns, and τ_{CR1} ~ 6 ns), the spectrum continues to decay even as the ratio becomes constant. From this spectral analysis, the yield of charge separation is ~5% for G-3 toward the end of the fsTA experiment and then decreases in keeping with the kinetic model. The low yield is also consistent with the SAS of the terminal state, which shows band inversion indicative of trapping at Sd (Figure 4a).

In contrast to EG-3, the fsTA data for EG-4 show 533 nm absorption within the first few ns, characteristic of a high yield of $Sd^{+\bullet}$. The strong amplitude of $Sd^{+\bullet}$ in EG-4 suggests more efficient hole transport through a GG-block than the AA-block,[4] and indicates that the hole is not trapped in the purine tract when in the presence of a deep hole site. In the model, the trapping step is combined with injection into the G_2 block. This is supported by the concomitant loss of the 460 nm $EG^{+\bullet}$ absorption with the appearance of the 533 nm $Sd^{+\bullet}$ band and

the lack of a strong apparent $G_2^{+\bullet}$ absorption.[20] Importantly, the characteristic absorption of the $EG^{+\bullet}$ species is observed prior to hole trapping by Sd, signifying that EG can serve as an optical tag of the hole location during transport. It is also possible, given the similar energetics of EG and G, that the hole is able to delocalize across GG and move as a polaron, such that there is only one observable population state. The electronic broad-ening associated with such polaron formation may also be suppressing the intensity of the 460 nm band in EG-4 relative to EG-3.[20]

The calculated yield of $Sd^{+\bullet}$ for EG-4 using eq 2 at 5 ns is Φ_{Sd} = 16%, compared to Φ_{CS} = 26% for G-4.[4] From eq 1, we calculate hole trapping times of τ_{Sd} = 4.4 and 2.2 ns for EG-4 and G-4, respectively, and hence, the kinetic model predicts similar yields of $Sd^{+\bullet}$ around 40% for EG-4 and G-4. The discrepancy is likely a result of comparison to a time-dependent quantum yield, as competitive charge recombination reduces the observable yield in the spectrum by depleting the $Sd^{+\bullet}$ population at a given observation time. In EG-4, the slower trapping rate is offset, in part, by the slower charge recombination of the $Sa^{-\bullet}/EG^{+\bullet}$ state, making the hole transfer to Sd more competitive. However, when the trapping rate is slowed substantially, as in the A_2 block case of EG-3, the kinetics become inverted, and the population of the trap state does not accumulate to measurable levels.

Despite the different oxidation potentials of EG and G and the slowing of overall charge transport, the observation of charge trapping at $Sd^{+\bullet}$ in reasonable yield for EG-4 demonstrates the utility of EG as a hole conduit. Comparison of the τ_{Sd} times for EG-4 and G-4 shows that hole transport from $EG^{+\bullet}$ is slower by a factor of 2, which manifests in a reduction of the trapping yield, though by less than a factor of 2 due to slowed charge recombination. The resultant yields are still moderate and easily detectable for optimized sequences, allowing for EG to be deployed in more complicated systems without large disruption of the dynamics. Additionally, we are able to directly observe the effect of the purine sequence on hole transport. In EG-3, the hole effectively stops at EG, as the inverted kinetics prevent meaningful population of the trap state from developing. However, if the sequence is designed properly, as in EG-4, the hole can easily be transported through the tract and arrive at Sd in reasonable yield, while its location is easily tracked and timed by the spectral tag on EG. We note that we also examined a system similar to EG-4 with an A_3-block in place of A_2 and observed no significant differences (data not shown), which suggests the behavior we have observed can be easily extended to larger diblock systems.

CONCLUSIONS

We have demonstrated the use of a phenylethynlguanine nucleobase to track the location of positive charge during photoinduced charge transport through DNA hairpins by means of transient absorption and femtosecond stimulated Raman spectroscopies. Following oxidation of EG, hole transport to $Sd^{+\bullet}$ through multiple Gs was observed, demonstrating the efficacy of EG to act as hole conduit in a G-tract. The addition of the phenylethynyl group appears to only slightly alter the oxidation potential of guanine, resulting in slowed hole transport through the poly(purine) sequence by a factor of 2, and subsequently ~30% lower trapping yields. However, the changes in the energy landscape are not so drastic as to severely alter the general hole transport behavior observed in transport through purine block sequences with unsubstituted guanine. We also examined the formation of $Sa^{-\bullet}$ by FSRS, which directly demonstrates reversible hole injection between ^{1}*Sa and the neighboring A-block.

Direct observation of EG as an intermediate hole acceptor demonstrates the utility of EG as a site-specific probe of hole migration and charge separation. Its unique electronic and vibrational spectral tags open the door to study hole migration and charge separation processes in complex DNA architectures such as 3-[44,45] and 4-way junctions,[46] or G-quadruplexes.[47] Furthermore, the use of EG to serve as a hole donor to both G and Sd demonstrates its ability to provide insight into hole transport through a G-tract. Future work to determine the hole mobility in mixed G(EG) sequences will seek to provide direct information on the hopping rates through G-tracts.[5] Optical detection of $G^{+\bullet}$ is complicated by its weak absorption that overlaps with features from other typical chromophores including the stilbene radical ions. Additionally, when the hole encounters a tract of Gs, it has been shown theoretically to delocalize across two or three Gs and behave as a polaron,[40] which broadens and weakens the signal, making it even more challenging to observe.[20] Even if $G_n^{+\bullet}$ is observed, its location within a larger G-tract cannot be easily determined. However, placement of EG at specific locations within larger runs of Gs would avoid this problem and assist in directly locating the hole during transit, with minimal alteration of the dynamics, and offer a promising route to exploring hole transport dynamics with site specificity.

ASSOCIATED CONTENT

* Supporting Information

Conjugate mass spectral data, thermal dissociation curves, electrochemical data, femtosecond/nanosecond transient absorption spectra, femtosecond stimulated Raman spectra, and data analysis, computational details, and Raman mode assignments (PDF)

AUTHOR INFORMATION

Corresponding Authors

*fdl@northwestern.edu
*ryan.young@northwestern.edu
*m-wasielewski@northwestern.edu

ORCID

Jiawang Zhou: 0000-0002-2399-0030
Frederick D. Lewis: 0000-0002-3669-2796
Ryan M. Young: 0000-0002-5108-0261
Michael R. Wasielewski: 0000-0003-2920-5440

Notes

The authors declare no competing financial interest.

ACKNOWLEDGMENTS

This research was funded by the U.S. Department of Energy, Office of Science, Office of Basic Energy Sciences, Chemical Sciences, Geosciences, and Biosciences Division under Awards DE-FG02-96ER14604 (F.D.L.) and DE-FG02-99ER14999 (M.R.W).

REFERENCES

(1) Lewis, F. D. Isr. J. Chem. 2013, 53, 350−365.
(2) Kawai, K.; Majima, T. Acc. Chem. Res. 2013, 46, 2616−2625.

(3) Fujitsuka, M.; Majima, T. Chem. Sci. 2017, 8, 1752−1762.
(4) Vura-Weis, J.; Wasielewski, M. R.; Thazhathveetil, A. K.; Lewis, F. D. J. Am. Chem. Soc. 2009, 131, 9722−9727.
(5) Conron, S. M. M.; Thazhathveetil, A. K.; Wasielewski, M. R.; Burin, A. L.; Lewis, F. D. J. Am. Chem. Soc. 2010, 132, 14388−14390.
(6) Kawai, K.; Kodera, H.; Osakada, Y.; Majima, T. Nat. Chem. 2009, 1, 156−159.
(7) Kawai, K.; Hayashi, M.; Majima, T. J. Am. Chem. Soc. 2012, 134, 9406−9409.
(8) Kawai, K.; Majima, T. Increasing the Hole Transfer Rate Through DNA by Chemical Modification. In Chemical Science of π-Electron Systems; Akasaka, T., Osuka, A., Fukuzumi, S., Kandori, H., Aso, Y., Eds.; Springer: Japan, 2015; pp 751−760.
(9) Thazhathveetil, A. K.; Vura-Weis, J.; Trifonov, A.; Wasielewski, M. R.; Lewis, F. D. J. Am. Chem. Soc. 2012, 134, 16434−16440.
(10) Steenken, S.; Jovanovic, S. V. J. Am. Chem. Soc. 1997, 119, 617−618.
(11) Lewis, F. D.; Kalgutkar, R. S.; Wu, Y.; Liu, X.; Liu, J.; Hayes, R. T.; Miller, S. E.; Wasielewski, M. R. J. Am. Chem. Soc. 2000, 122, 12346−12351.
(12) Geacintov, N. E.; Solntsev, K.; Johnson, L. W.; Chen, J.; Kolbanovskiy, A. D.; Liu, T.; Shafirovich, V. Y. J. Phys. Org. Chem. 1998, 11, 561−565.
(13) Yun, B. H.; Lee, Y. A.; Kim, S. K.; Kuzmin, V.; Kolbanovskiy, A.; Dedon, P. C.; Geacintov, N. E.; Shafirovich, V. J. Am. Chem. Soc. 2007, 129, 9321−9332.
(14) Genereux, J. C.; Barton, J. K. Chem. Rev. 2010, 110, 1642−1662.
(15) Schuster, G. B. Acc. Chem. Res. 2000, 33, 253−260.
(16) Giese, B. Acc. Chem. Res. 2000, 33, 631−636.
(17) Candeias, L. P.; Steenken, S. J. Am. Chem. Soc. 1989, 111, 1094−1099.
(18) Wu, L.; Liu, K.; Jie, J.; Song, D.; Su, H. J. Am. Chem. Soc. 2015, 137, 259−266.
(19) Kobayashi, K.; Yamagami, R.; Tagawa, S. J. Phys. Chem. B 2008, 112, 10752−10757.
(20) Harris, M. A.; Mishra, A. K.; Young, R. M.; Brown, K. E.; Wasielewski, M. R.; Lewis, F. D. J. Am. Chem. Soc. 2016, 138, 5491− 5494.
(21) Lewis, F. D.; Wu, T. F.; Liu, X. Y.; Letsinger, R. L.; Greenfield, S. R.; Miller, S. E.; Wasielewski, M. R. J. Am. Chem. Soc. 2000, 122, 2889−2902.
(22) Wu, Y.-L.; Brown, K. E.; Gardner, D. M.; Dyar, S. M.; Wasielewski, M. R. J. Am. Chem. Soc. 2015, 137, 3981−3990.
(23) Lewis, F. D.; Zhu, H.; Daublain, P.; Fiebig, T.; Raytchev, M.; Wang, Q.; Shafirovich, V. J. Am. Chem. Soc. 2006, 128, 791−800.
(24) Lewis, F. D.; Wu, Y.; Zhang, L.; Zuo, X.; Hayes, R. T.; Wasielewski, M. R. J. Am. Chem. Soc. 2004, 126, 8206−8215.
(25) Seidel, C. A. M.; Schulz, A.; Sauer, M. H. M. J. Phys. Chem. 1996, 100, 5541−5553.
(26) El-Yazbi, A. F.; Palech, A.; Loppnow, G. R. J. Phys. Chem. A 2011, 115, 10445−10451.
(27) Santoro, F.; Improta, R.; Fahleson, T.; Kauczor, J.; Norman, P.; Coriani, S. J. Phys. Chem. Lett. 2014, 5, 1806−1811.
(28) Lewis, F. D.; Zhang, L.; Liu, X.; Zuo, X.; Tiede, D. M.; Long, H.; Schatz, G. C. J. Am. Chem. Soc. 2005, 127, 14445−14453.
(29) Johnson, W. C. CD of Nucelic Acids. In Circular Dichroism, Principles and Applications; Berova, N., Nakanishi, K., Woody, R. W., Eds.; Wiley-VCH: New York, 2000; pp 741−768.
(30) Kypr, J.; Kejnovska, I.; Renciuk, D.; Vorlíckova, M. Nucleic Acids Res. 2009, 37, 1713−1725.
(31) Trantírek, L.; Stefl, R.; Vorlíckova, M.; Koca, J.; Sklenarar, V. r.; Kypr, J. J. Mol. Biol. 2000, 297, 907−922.
(32) Young, R. M.; Singh, A. P. N.; Thazhathveetil, A. K.; Cho, V. Y.; Zhang, Y.; Renaud, N.; Grozema, F. C.; Beratan, D. N.; Ratner, M. A.; Schatz, G. C.; Berlin, Y. A.; Lewis, F. D.; Wasielewski, M. R. J. Am. Chem. Soc. 2015, 137, 5113−5122.
(33) Lewis, F. D.; Wu, T.; Liu, X.; Letsinger, R. L.; Greenfield, S. R.; Miller, S. E.; Wasielewski, M. R. J. Am. Chem. Soc. 2000, 122, 2889− 2902.
(34) We note that a true species-associated spectrum by definition cannot represent a mixture of states, but for simplicity our model neglects the short-lived populations of the coexcited species. In this way, the SAS here (at least at early times) may be better referred to as decay-associated spectra where the evolution is described by the solutions to the kinetic model defined in the text. However, after the first ~100 ps, the contribution from the other short-lived states is minimal and the spectra are well-described as species-associated.
(35) Singh, A. P. N.; Harris, M. A.; Young, R. M.; Miller, S. A.; Wasielewski, M. R.; Lewis, F. D. Faraday Discuss. 2015, 185, 105−120.
(36) Sumitani, M.; Yoshihara, K.; Nagakura, S. Bull. Chem. Soc. Jpn. 1978, 51, 2503−2507.
(37) Lewis, F. D.; Liu, X.; Wu, Y.; Miller, S. E.; Wasielewski, M. R.; Letsinger, R. L.; Sanishvili, R.; Joachimiak, A.; Tereshko, V.; Egli, M. J. Am. Chem. Soc. 1999, 121, 9905−9906.
(38) Middleton, C. T.; de La Harpe, K.; Su, C.; Law, Y. K.; Crespo-Hernandez, C. E.; Kohler, B. Annu. Rev. Phys. Chem. 2009, 60, 217− 239.
(39) Kochman, M. A.; Pola, M.; Miller, R. J. D. J. Phys. Chem. A 2016, 120, 6200−6215.
(40) Renaud, N.; Berlin, Y. A.; Lewis, F. D.; Ratner, M. A. J. Am. Chem. Soc. 2013, 135, 3953−3963.
(41) Renaud, N.; Berlin, Y. A.; Ratner, M. A. Proc. Natl. Acad. Sci. U. S. A. 2013, 110, 14867−14871.
(42) Renaud, N.; Harris, M. A.; Singh, A. P. N.; Berlin, Y. A.; Ratner, M. A.; Wasielewski, M. R.; Lewis, F. D.; Grozema, F. C. Nat. Chem. 2016, 8, 1015−1021.
(43) Lewis, F. D.; Liu, J.; Zuo, X.; Hayes, R. T.; Wasielewski, M. R. J. Am. Chem. Soc. 2003, 125, 4850−4861.
(44) Sabir, T.; Toulmin, A.; Ma, L.; Jones, A. C.; McGlynn, P.; Schröder, G. F.; Magennis, S. W. J. Am. Chem. Soc. 2012, 134, 6280− 6285.
(45) Santhosh, U.; Schuster, G. B. Nucleic Acids Res. 2003, 31, 5692−5699.
(46) Lake, A.; Shang, S.; Kolpashchikov, D. M. Angew. Chem., Int. Ed. 2010, 49, 4459−4462.
(47) Thazhathveetil, A. K.; Harris, M. A.; Young, R. M.; Wasielewski, M. R.; Lewis, F. D. J. Am. Chem. Soc. 2017, 139, 1730−1733.